Redefinition of the active species and the mechanism of the oxygen evolution reaction on gold oxide

Yang, S.; Hetterscheid, D.G.H.

Note: To cite this publication please use the final published version (if applicable).

Redefinition of the Active Species and the Mechanism of the Oxygen Evolution Reaction on Gold Oxide

Shengxiang Yang and Dennis G. H. Hetterscheid*

Read Online

ACCESS | Metrics & More | Article Recommendations | Supporting Information

ABSTRACT: Accurately identifying the active species of catalytic materials and understanding how they catalyze the oxygen evolution reaction (OER) are critical for the development of energy storage technologies. In this contribution, we identify two pH-dependent active oxides by mapping the reduction behavior of gold oxide and by in situ surface-enhanced Raman spectroscopy. It was found that α-oxide is preferentially formed in an acidic solution, whereas β-oxide, $Au(OH)_3$, is preferably formed in an alkaline solution. In line with the presence of two different surface structures on gold, there are two OER mechanisms: one mechanism wherein water splitting occurs via proton-coupled electron-transfer steps mediated by α-oxide and the other mechanism wherein electron transfer and proton transfer are decoupled and mediated by a deprotonated form of $Au(OH)_3$. This identification of pH-dependent oxides offers a different perspective in our understanding of the OER mechanism on metal oxides in a full pH scale range.

KEYWORDS: electrocatalysis, oxygen evolution reaction, oxide reduction, gold electrochemistry, proton-coupled/decoupled electron transfer
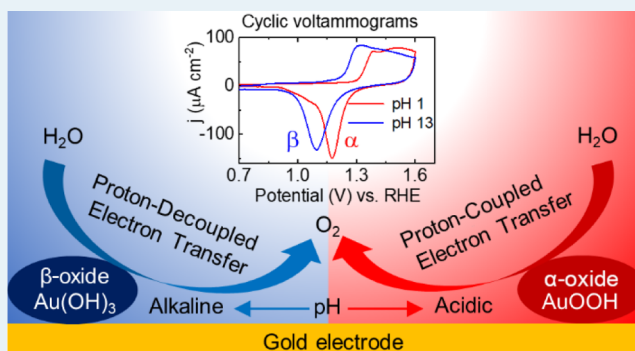
1. INTRODUCTION

More than 230 years ago, the first water electrolysis experiment was carried out by evolving hydrogen and oxygen separately at two gold electrodes.[1,2] At present, water splitting is considered as an ideal solution to the world's renewable energy storage problem.[3−5] Using sunlight to split water into hydrogen and oxygen allows for the conversion of solar energy to chemical energy. This energy can be converted back to electricity in a fuel cell. It is widely accepted that one of the key bottlenecks in the overall water splitting reaction is the slow kinetics of the catalytic water oxidation reaction taking place at the anode.

Metal oxides are considered the best and most stable electrocatalysts for water oxidation.[3,6,7] In general, oxidation mechanisms of noble metals involve three stages: (a) two-dimensional electrodeposition of OH and O species on the metal surface, (b) quasi-three-dimensional (quasi-3D) surface reconstruction and place exchange between the OH or O species and surface metal atoms, and (c) growth or thickening of the oxide film.[8] Further development of the oxide film formation includes thin oxide films by stages (a) and (b) and thick hydrous oxide films by extension of oxide growth beyond the monolayer level.[9] These mechanistic models are crucial not only for guiding catalyst design[10,11] but also for our understanding of the oxygen evolution reaction (OER) mechanism on metal oxides.[6,12]

The initial quasi-3D metal oxide formation proceeding via reconstruction and place exchange was not only identified on the basis of electrochemical behavior[8,13] but also directly observed by atomic-resolution scanning tunneling microscopy and surface structure analyses.[14,15] However, these in situ observations and surface analysis techniques become less useful in the discussion of thicker oxide film formation because these metal oxide layers are typically highly disordered.[16] Despite the lack of an effective detection of the surface structure of thicker oxide films, a concept of so-called hydrous oxide films involving thicker oxide formation was put forward on the basis of the observation that separate reduction peaks can be observed upon reduction of the metal oxide.[8,9] In these reports, the separation of the metal oxide reduction peaks was assumed to correspond to the reduction of the inner monolayer and the outer hydrous layer of the metal oxide surfaces.

In this article, we return to gold, the electrode material originally used 230 years ago, and demonstrate that the model of inner and outer hydrous oxide films is incorrect. We identify that different active species, whose formations are pH-dependent, play a role by combining the observed reduction
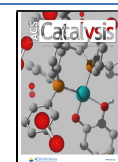
behavior of gold oxide and in situ surface-enhanced Raman spectroscopy (SERS). Identification of this pH-dependent oxide is critical in order to fully understand the OER mechanism.

A typical and conventional OER mechanism on a metal oxide surface involves four proton-coupled electron-transfer (PCET) steps at the oxide−electrolyte interface.[7,17] The PCET-OER mechanism emphasizes the importance of optimizing the binding strength of reaction intermediates on surfaces to get high OER activities, which allows one to make OER activity predictions according to electronic structure parameters of the metal oxide.[4,18] However, the PCET-OER mechanism is not necessarily correct in all cases. OER activities that depend on the pH on the reversible hydrogen electrode (RHE) scale have been observed for various metal oxides in alkaline environments,[19−21] indicating that the OER process follows electron-transfer steps that are not coupled to proton transfer on these metal oxides. The origin of pH-dependent OER mechanisms on the RHE scale has been revealed in recent years. For example, high-index facets of polycrystalline surfaces on oriented RuO_2 surfaces,[22] deprotonation of Ni-based catalysts,[23] and the covalence of metal−oxygen bonds in perovskites[21] can cause pH-dependent OER activity on the RHE scale. Moreover, many other explanations regarding OER mechanisms are only consistent in a relatively narrow pH range.[6,21,23] Although the difference in OER activity in acidic and alkaline solutions is often related to the acid−base characteristics of the surface,[17,24] the lack of a clear explanation for these so-called "acid−base characteristics" limits our understanding of water splitting in a full pH range. In this article, we show that the mechanism wherein OER occurs on gold depends strongly on the surface structure of gold oxide and that proton transfer and electron transfer are coupled under acidic conditions, whereas these are decoupled during OER under alkaline conditions.

2. EXPERIMENTAL SECTION

2.1. General. All glassware was thoroughly cleaned to remove impurities by overnight submersion in an aqueous 0.5 M H_2SO_4 solution mixed with 6.3 mM $KMnO_4$, followed by removal of excess $KMnO_4$ on the glassware in diluted H_2SO_4 and H_2O_2. The glassware was subsequently rinsed five times and boiled two times in Millipore MilliQ water (resistivity = 18.2 MΩ cm). Prior to the electrochemical experiment, the glassware was boiled once in MilliQ water. Alumina suspensions (1.0, 0.3, and 0.05 μm) were obtained from Buehler. Electrolyte solutions were prepared with Suprapur (Merck) reagents and MilliQ water. pH measurements were done using a Hanna Instruments HI 4222 pH meter which was calibrated using IUPAC standard buffers.

2.2. Electrochemical Measurements. All electrochemical measurements were conducted with Autolab PGSTAT 12, 204, and 128 N potentiostats in combination with Autolab NOVA software and carried out in conventional single-compartment three-electrode glass cells at around 25 °C. A polyether ether ketone (PEEK)-encapsulated gold electrode (A = 0.0314 cm², Metrohm) was used as the working electrode, and a gold wire was the counter electrode, while an RHE was employed as the reference electrode. Before every experiment, the working electrode (PEEK-encapsulated gold) was manually polished for 2 min with 1.0, 0.3, and then 0.05 μm alumina suspensions on Buehler cloth polishing pads, followed by sonication in MilliQ water for 10 min. At the same time, the

counter electrode (the gold wire) was flame-annealed and rinsed with MilliQ water. The reference electrode (RHE) consisting of a Pt wire was connected via a Luggin capillary and continuously bubbled with H_2 gas during the measurement.

The concentration of the electrolyte solution was kept at 0.1 M for different pH solutions from pH 1−13 obtained by mixing 0.1 M H_2SO_4, NaOH, and Na_2SO_4. Unless stated otherwise, pH 1−13 represent solutions with a fixed pH value comprising H_2SO_4, NaOH, or Na_2SO_4 in this article. Dissolved oxygen in the solution was removed prior to measurements by aeration with argon (a purity grade of 5.0) for at least 30 min. Argon was kept flowing above the solution during experiments. The onset potential of OER is obtained by intersection of tangents between the baseline and the rising current in the positive scan of cyclic voltammograms, as shown in Figure S1.[25] Tafel analysis was done under steady-state conditions and was used to understand the OER mechanism (see Figure S10a,b).[26]

2.3. In Situ Surface-Enhanced Raman Spectroscopy. In situ SERS was performed using a confocal Raman microscope (LabRamHR, HORIBA Yobin Yvon) with an Olympus 50× microscope objective, which was not immersed in the electrolyte, into a 5 μm spot on the electrode surface, which has been documented previously.[6,27,28] Backscattered light was filtered using a 633 nm edge filter, directed to the spectrograph and to the detector. With this configuration, a resolution of 1.2 cm^{-1} was obtained.[29] The electrochemical SERS experiments were performed with an Ivium potentiostat/galvanostat (IviumStat). Figure S2 shows a schematic diagram of the electrochemical setup for in situ surface-enhanced Raman spectroscopic measurements. Each SERS analysis was performed with the accumulation of 100 scans with a 1 s collection time.

A roughened gold surface was used as the working electrode. The working electrode was mechanically polished to a mirror finish using alumina with different grain sizes to 0.05 μm, rinsed with MilliQ water, and sonicated for 15 min to remove all residuals of mechanical polishing. Then, the gold electrode was electrochemically roughened by 25 oxidation−reduction cycles (ORCs) in a 0.1 M solution of KCl. The ORCs were performed between −0.30 and 1.20 V versus the saturated calomel electrode, which were held for 30 and 1.3 s, respectively. A brownish surface was formed after roughening gold by this method.[6,30] The quality of Au roughing can be visualized by a comparison of the current of the cyclic voltammogram before and after Au roughing, as shown in Figure S3. SERS spectra were recorded at 1 V versus RHE and set as the background signal and subtracted from further measurements in the same solution. Different backgrounds were set for solutions of different pH (H_2SO_4, Na_2SO_4, and NaOH). All data were processed using OriginPro 9.1.

3. RESULTS AND DISCUSSION

3.1. Inconsistencies in Conventional Models for the Electrochemical Redox Behavior of Gold. In a typical cyclic voltammogram of gold (Figure 1a), the most notable oxide formation response in the positive sweep is an extended plateau rather than sharp peaks, independent of the applied pH. The formation of this plateau is attributed to the increased energy required to generate additional oxide by gradual changes in the hysteresis of the oxidation potential between Au and Au−OH species in the oxide layer.[31] It is therefore difficult to investigate the gold oxidation chemistry through
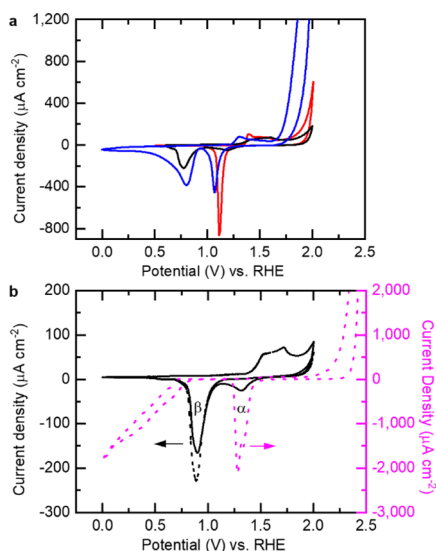
Figure 1. Electrochemical redox behavior of gold. (a) Cyclic voltammograms of gold between 0 and 2 V vs RHE at 50 mV/s in Ar-saturated 0.1 M H_2SO_4 (red line), Na_2SO_4 (black line), and NaOH (blue line). (b) Cyclic voltammograms of gold vs RHE in an Ar-saturated 0.1 M Na_2SO_4 solution. Scan range of cyclic voltammograms: 0−2 V (black line); 0−2.7 V (pink dotted line); black dotted line: gold was first oxidized between 1.6 and 1.8 V vs RHE for 200 s, prior to recording the cyclic voltammogram between 0 and 2 V vs RHE in fresh 0.1 M Na_2SO_4 solution.

this continuous oxidation process in the positive sweep. The behavior of gold in the negative sweep is more indicative of the processes taking place at its surface. Only one reduction peak can be detected in the acidic solution, while the reduction peak splits into two separated peaks upon increasing the pH. Stable gold oxide with a +III oxidation state can be formed by the reaction $2Au + 3H_2O \rightarrow Au_2O_3 + 6H^+ + 6e^-$, $E^O = 1.46$ V, which is illustrated by the Pourbaix diagram of gold. Gold oxide with a +IV oxidation state can only be formed at a very high electric field by the reaction $2Au + 4H_2O \rightarrow 2AuO_2 + 8H^+ + 8e^-$, $E^O = 4.14$ V.[32,33] Consequently, Au(III) is the only oxidation state of gold present in the gold oxide layers as was shown by ex situ X-ray photoelectron spectroscopy[34] and in situ extended X-ray absorption fine-structure studies.[35] Because only one oxidation state (the trivalent oxidation state) is involved, the presence of more than one reduction peak cannot be explained by different oxidation states of gold.

On the basis of the "separated reduction peaks" that can be observed for gold, the concept of hydrous oxide films was put forward last century.[9,36,37] The two main gold oxide reduction peaks have historically been assigned to a compact inner monolayer oxide and a hydrous outer layer oxide. In the acidic solution, the hydrous outer oxide layer was suggested to be thin enough so that its reduction peak overlaps with the reduction peak of compact inner oxides. At higher pH, the thicker hydrous outer oxide layer was proposed to cause the reduction peak to split into two peaks (Figure 1a).[31] The trivalent oxidation state of gold in all oxide forms has been regarded as consistent with the inner and outer layer oxide model.

However, there are major problems with the inner and outer hydrous oxide model. In a cyclic voltammogram of gold at neutral pH (black line in Figure 1b), the relatively positive reduction peak corresponds to the inner monolayer of oxide,

named α-oxide, and the relatively negative reduction peak is assigned to the outer hydrous oxide, named β-oxide. According to the mechanism of hydrous oxide film formation, the α-peak cannot disappear because it represents the inner structure of the oxide layers. However, only the β-peak, that is, no α-peak, can be detected on an oxidized gold electrode, which is oxidized at 1.6−1.8 V versus RHE in advance (black dotted line in Figure 1b). Moreover, when the upper limit of the positive scan is extended from 2.0 to 2.7 V (pink dotted line in Figure 1b), the α-peak increases to a huge reduction peak; this is not at all in line with the hydrous oxide film model, where the α-peak should not change in magnitude because it is supposed to correspond to an inner monolayer.

Figure 2a shows the change of cyclic voltammograms for gold with the increase of the upper vertex potential in acidic, neutral, and alkaline solutions. A new reduction peak appears once the upper limit of the voltammetry experiment is set above the onset potential of OER. In order to further identify the γ-peak, the electrochemistry of gold was recorded in acidic, neutral, and alkaline solutions with an RDE, as shown in Figure 2b. It is clearly shown that the γ-peak disappears upon rotation, while the reduction peaks of gold oxide do not significantly change once O_2 is removed at a high rotation rate. This implies that the γ-peak is the result of the reduction of O_2. Note that the γ-peak in alkaline solutions is often misinterpreted as a β-peak of gold oxide reduction in the literature,[31,37,38] which makes the discussion of the redox chemistry of gold much more complex.

In order to eliminate the interference of O_2, cyclic voltammograms of gold were recorded as a function of pH by keeping the upper limit of the cyclic voltammogram at the potentials at which gold oxidation begins while still below the onset potential of OER (Figure 3a). Both the α- and β-peaks were detected in all solutions irrespective of the pH. The cyclic voltammograms in the alkaline solution revealed that β-oxide is formed first while the applied potential is kept well below the
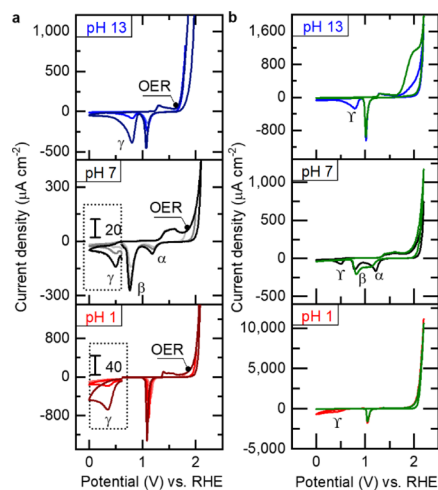
Figure 2. Recognition of the γ-peak being associated with oxygen reduction. (a) Cyclic voltammograms of gold vs RHE at 50 mV/s with change of scan range in the Ar-saturated solution; the γ-peaks are amplified (by different multiples) to clearly show their position; (b) cyclic voltammograms on a gold rotating disk electrode (RDE) at 0 rpm between 0 and 2.2 V vs RHE in Ar-saturated solutions of pH 1 (red line), pH 7 (black line), and pH 13 (blue line). Green line: cyclic voltammograms of the RDE with 3000 rpm at these different pH solutions.
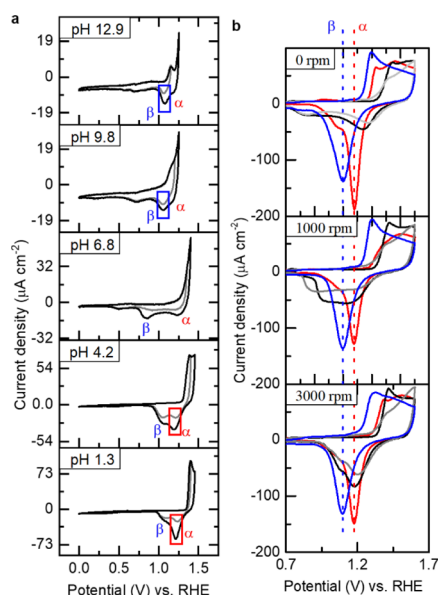
Figure 3. Identification of active gold oxides. (a) Cyclic voltammograms of gold in different Ar-saturated pH solutions at 50 mV/s. The upper limit of the cyclic voltammogram is kept to the range of potentials where gold oxidation occurs. (b) Cyclic voltammograms of gold (RDE) between 0 and 1.6 V vs RHE at rotation rates with different Ar-saturated 0.1 M electrolytes: H_2SO_4 (red line), Na_2SO_4 (black line), $NaClO_4$ (gray line), and NaOH (blue line). The exact change of the potential value as a function of the rotation speed is shown in Figure S4.

reduction potential of α-oxide; this is contrary to the past hydrous oxide films model wherein the inner α-oxide must form first. Furthermore, a larger α-peak was found in an acidic

solution, while the β-peak was significantly larger under alkaline conditions. This implies that α- and β-oxides are two relatively independent forms of gold oxide, whose formation is dependent on the pH. A similar result is obtained when the solution was changed from a Na_2SO_4 solution to a $NaClO_4$ solution, which implies that there is little influence of the electrolyte (Figure S5).

3.2. Redefinition of the Active Gold Oxides. The initial stage of gold oxidation has been extensively discussed in the past.[8,13] The hydroxide ion under alkaline conditions and water under acidic conditions first chemisorb on gold to form $Au-OH_{ads}$. $Au-OH_{ads}$ would continue to convert to $Au(OH)_3$ by place-exchange reactions between Au and OH^-. The initial gold oxide $Au(OH)_3$ formation is in good agreement with density-functional theory (DFT)-based computational studies of the surface thermodynamics of electrochemistry of gold.[6] Because $Au(OH)_3$ relies on place-exchange reactions between Au and OH^-, $Au(OH)_3$ formation should be enhanced with the increase of the pH. From a comparison of cyclic voltammograms at different pH (Figure 3a), the β-peak therefore most likely corresponds to the reduction of $Au(OH)_3$. Actually, gold(III) precipitations in alkaline media have been shown to correspond to $Au(OH)_3$ but not $Au_2O_3 \cdot nH_2O$ according to X-ray diffraction, transmission electron microscopy, Au Mössbauer spectroscopy, X-ray absorption spectroscopy, and thermogravimetry/differential thermal analysis studies.[39]

It is interesting to note that the reduction potential difference of α- and β-oxide is roughly 0.13 ± 0.01 V in both acid and alkaline solutions but becomes more than 0.4 V under neutral conditions (0.42 V at pH 6.8). Therefore, RDE experiments were conducted with varying rotation rates (Figure 3b). At 0 rpm, there is a minor positive shift of the
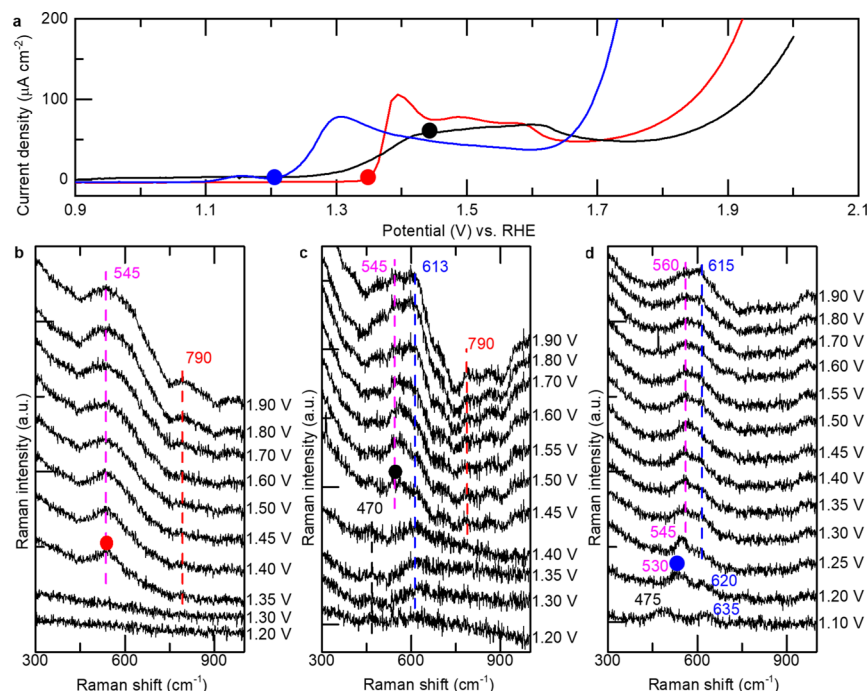
Figure 4. In situ SERS of gold oxidation. (a) LSV for electrocatalytic water oxidation from 0.9 to 2 V vs RHE at 50 mV/s on the gold electrode in Ar-saturated 0.1 M H_2SO_4 (red line), Na_2SO_4 (black line), and NaOH (blue line) solution. (b–d) SERS of gold oxidation in 0.1 M H_2SO_4 (b), Na_2SO_4 (c), and NaOH (d). Oxidation potentials were recorded on the RHE scale. Solid circles represent the points where the $\nu(Au-O)$ vibration becomes visible in 0.1 M H_2SO_4 (red circle), Na_2SO_4 (black circle), and NaOH (blue circle) solutions.

α-peak and a clear negative shift of the β-peak in the neutral solution compared to that in both acidic and alkaline media irrespective of whether Na_2SO_4 or $NaClO_4$ was used as an electrolyte. The potential shifts of the α- and β-peaks in neutral media can be avoided upon increasing the rotation rates of the gold electrode. At 3000 rpm, it is clearly shown that the peak positions of α- and β-oxide in the neutral solution coincide with the peak position of α in the acid and the position of β in the base. An effect of the scan rate on the peak position of the reduction peaks was investigated (Figure S6). Both oxide reduction peaks show only a minor negative potential shift with the increase of the scan rate. Their currents are linearly dependent on the scan rate, which is fully consistent with the characteristics of an irreversible oxide reduction process on the gold surface.

In situ SERS was performed to further identify the structure of α- and β-oxide. The potential-dependent vibrational spectra in 0.1 M H_2SO_4, Na_2SO_4, and NaOH solution are shown in Figure 4b−d. The observed broad frequency bands at 530−565 cm^{-1} are characteristic of the $\nu(Au-O)$ vibration, which can be detected when the applied potential is set above 1.35 V in H_2SO_4 1.45 V in Na_2SO_4 and 1.2 V in NaOH. These oxidation potentials are also consistent with the potential where gold oxidation occurs in linear sweep voltammetry (LSV) measurements (Figure 4a). The $\nu(Au-O)$ vibration may point to oxide formation, although the band is especially broad and its frequency is easily influenced by, for example, absorption of the electrolyte (Figure S7), and/or the applied potential.[40] The wide Raman bands are most likely due to different coordination geometries and hydration states of the gold surface.[41]

The normal surface electro-oxidation of noble metals includes two steps: (i) initial deposition of O or OH species and (ii) "oxide film" formation by place exchange with the surface metal atoms and adsorbed oxygen species along with further electron transfer.[8] These two steps cannot be clear-cut distinguished. A band around 470−475 cm^{-1} is assigned to the reversible adsorbed OH$^-$ (Figure 4c,d). The $\nu(Au-OH^-)$ occurs around 400−450 cm^{-1} in 1 M KOH according to the literature and shifts to higher frequencies at more positive potentials.[41] A significant frequency change from $\nu(Au-OH^-)$ at 475 cm^{-1} at 1.1 V to higher $\nu(Au-O)$, 530−560 cm^{-1}, with more positive potentials in NaOH indicates a change in the oxide formation process from step (i) to step (ii). This is explained by yielding a strong ionic component to the Au−O bond energy in the process of place exchange between gold and oxygen because these gold atoms would get a more positive formal oxidation state.[41] According to the Raman spectrum of bulk-phase solid $Au(OH)_3$, the $\nu(Au-OH)$ vibration of $Au(OH)_3$ should be observed at 635 cm^{-1}.[41] Interestingly, the $\nu(Au-OH)$ vibration of $Au(OH)_3$ at 635 cm^{-1} first occurs at 1.1 V in NaOH and has a minor shift to 613 cm^{-1} with higher oxidation potentials (Figure 4d). Note that the $\nu(Au-OH)$ vibration at 613 cm^{-1} can also be observed in a Na_2SO_4 solution (Figure 4c). This is consistent with the occurrence of the β-peak in cyclic voltammograms of gold (Figure 3) caused by the reduction of $Au(OH)_3$.

In addition, the absence of an α-peak in the cyclic voltammogram in an NaOH solution (Figure 3a) is fully in line with the absence of a signal around 800 cm^{-1} in SERS experiments (Figure 4d). Therefore, we assume that the Raman signals recorded at approximately 820 cm^{-1} in

perchloric media and at 790 cm^{-1} in sulfuric media are related to α-oxide (Figure S7).

In previous studies, this band was found at values between 810 and 827 cm^{-1} in perchloric media.[6,40,42] A minor shift of 3−4 cm^{-1} was observed upon substitution of H_2O for D_2O.[40,42] A significant shift of 74−77 cm^{-1} was observed upon substitution of $H_2^{16}O$ for $H_2^{18}O$ in previous isotope studies.[6] Furthermore, the assignment of bands around 820 cm^{-1} to other forms of oxygen associated with Au (e.g., superoxo, oxo, and hydroxy) was excluded based on a series of DFT calculations.[27,42] Therefore, the signals in the range of 810 ± 20 cm^{-1} must be assigned to O−OH stretching. The O−OH stretching appears simultaneously with the appearance of $\nu(Au-O)$ of gold oxide in a H_2O_2 decomposition experiment on gold nanoparticles.[42] Tian and co-workers therefore claimed that the peak around 800 cm^{-1} must be assigned to an O−O stretch of a H-containing reaction intermediate and not simply to an O−O stretch of peroxide. Interestingly, two independent research groups (Bell and Koper) have claimed that the vibrational signal around 800 cm^{-1} was observed at least 0.4 V less positive than the onset of water oxidation in their in situ SERS experiments.[6,40] However, according to DFT calculations of *OOH on gold and other metal oxide surfaces, the *OOH intermediate is the highest-energy intermediate and should rapidly decompose into O_2.[7,43] An explanation is that peroxidic species may exist within the oxide layer in the acidic solution, which is probably somehow related to a highly nonordered structure.[19] However, this still cannot explain the lack of an *OOH SERS signal in a low oxidation potential range in the alkaline solution. Thus far, these Raman signals have not been investigated in a full pH range. Koper and co-workers have put forward a more stable oxyhydroxide (AuOOH) formation mechanism in acidic solutions on the basis of DFT calculations. The oxyhydroxide is proposed to play an important role in the OER process. We therefore do consider the possibility that α-oxide may predominantly be an oxyhydroxide, whose structure may include *OOH species within the oxide layer. In order to further confirm the relationship between α-oxide and $\nu(OOH)$, an in situ SERS reversibility experiment was carried out in a neutral solution (Figure 5), where the collection time
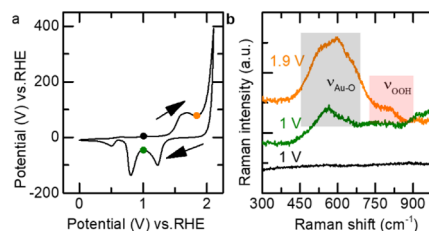
Figure 5. Reversibility of SERS of gold oxidation in 0.1 M Na_2SO_4. (a) Cyclic voltammogram of the gold electrode at 50 mV/s. (b) SERS of gold oxidation in a positive scan and negative scan of the cyclic voltammogram.

of SERS signals was increased from 1 to 10 s to trace the change of SERS. Here, $\nu(Au-O)$ in the range of 500−620 cm^{-1} and $\nu(OOH)$ at 790 cm^{-1} can be detected once the potential is increased from 1 to 1.9 V. When the potential is decreased from 1.9 to 1 V, the $\nu(OOH)$ will disappear, while some of the $\nu(Au-O)$ signal remains. At this potential of 1 V, only β-oxide can exist, while α-oxide is reduced. This confirms that the signal around 800 cm^{-1} does not simply represent

surface-bound hydroperoxide species as an intermediate of OER yet somehow must be related to the existence of α-oxide.

3.3. Two OER Mechanisms Led by Two Gold Oxides.
Our results show that the structure of gold oxide is strongly dependent on the pH of the solution: α-oxide is preferentially formed in an acidic solution and β-oxide, Au(OH)$_3$, is preferentially formed in an alkaline solution (Figure 6a). As
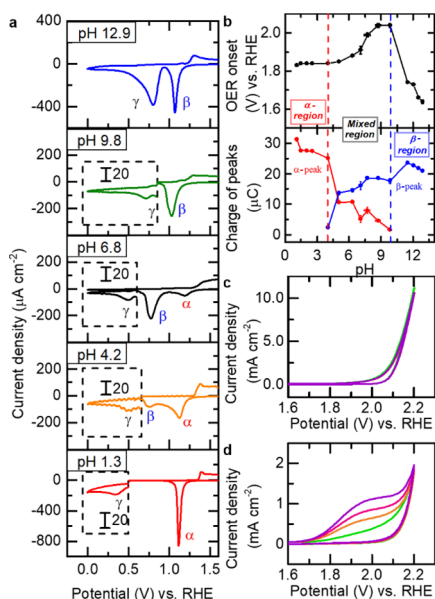
Figure 6. pH-dependent oxide formation and OER activity on gold. (a) Cyclic voltammograms of the gold electrode showing the reduction peaks at 50 mV/s in different Ar-saturated pH solutions. Note that the scan range is 0−2 V vs RHE. The γ-peaks are amplified (by different multiples) to clearly show their position. The oxidative areas in the 1.5−2 V range of these cyclic voltammograms, showing OER, are shown in Figure S8. (b) Onset potential of OER (top) and the integrated charges of the α- and β-oxide reduction peaks at 50 mV/s in Ar-saturated solutions are plotted as a function of pH. The error bars represent the standard deviation of three measurements. (c−d) Cyclic voltammograms of gold (RDE) at 50 mV/s in Ar-saturated 0.1 M H$_2$SO$_4$ (b) or NaOH (c) solution at different rotation rates: 0 rpm (green line), 100 rpm (orange line), 1000 rpm (pink line), and 3000 rpm (violet line); the scan range is 0−2.2 V vs RHE.

with the surface structure of gold oxide, the mechanism of OER is also affected by the solution pH. The OER activity increases with decreasing pH in the low-pH region and with increasing pH in the high-pH region (Figure S8). Very similar results have been obtained by Stahl and co-workers, who revealed that different cobalt-based active species exist at different pH values and have investigated the OER mechanism in a full pH region.[26] Although such pH-dependent species may exist on more metal-based catalysts, the lack of a clear understanding of the mechanism of pH-dependent active species limits the development of better OER catalysts in the case of several more metal-based systems.

Figure 6b shows the OER onset potential and the integrated charges of the α- and β-oxide reduction peaks in a full pH window. The pH environment can be divided into three different regions: (1) the α-region (pH lower than 4) in the acidic solution, (2) the mixed region (pH from 4 to 10) in the neutral solution, and (3) the β-region (pH higher than 10) in the alkaline solution. In the α-region, α-oxide is the only oxide that can exist in a stable form. In this window, the OER onset

potential is fixed at 1.84 V versus RHE. This pH-independent OER activity on the RHE scale in the α-region implies that the OER process at α-oxide proceeds via four PCET steps. In the mixed region, both α-oxide and β-oxide exist on the electrode surface. The amount of the two oxides changes with the pH of the solution in this region. The amount of α-oxide decreases, while the amount of β-oxide increases with the increase of the pH. Interestingly, the OER onset potential also increases with pH. This shows that β-oxide is less active for OER than α-oxide in this pH window. The OER activity level therefore strongly relies on the existence of α-oxide in this mixed oxide region. In the β-region at high pH values, only β-oxide is present at the electrode surface. In this pH window, the OER onset potential gradually decreases with an increase of the pH. This implies that OER must be pH-dependent when catalyzed by β-oxide, which implies that some of the proton- and electron-transfer steps are decoupled in the OER process in the high pH region. For a reaction, the proton-transfer step and electron-transfer step will decouple if one of their activation energies is smaller than the activation energy of the PCET process.[17]

In order to further evaluate the relationship between OER activity and the existence of oxides, a series of Tafel plots are obtained for these different pH regimes (Figure S9 and Table S1). In the α-region, all Tafel plots overlap with Tafel slopes that are around 120 mV/decade. This further confirms that OER at α-oxide proceeds via a pH-independent process. In the mixed region, the Tafel slopes are up to around 160−190 mV/decade, which is in agreement with a lower OER activity in this pH window. However, the Tafel plots of β-oxide appear initially at different potential regions and show that the evolution of oxygen starts earlier once the solution pH increases in the β-region. This is fully in line with a pH-dependent OER process. Moreover, lower Tafel slopes (60−70 mV/decade) are found in the β-region, which implies that the decoupled OER process has a higher efficiency for oxygen evolution compared to the PCET-OER process on α-oxide.

The effect of solution pH on the proton affinity and electron affinity of the catalyst or reactant has been discussed in recent years.[17,19,44] According to acid−base characteristics of a catalyst on the surface, some catalysts have a proton affinity, which is equal to the (surface) pK_a of the acid dissociation constant. If a solution pH is higher than the (surface) pK_a of a catalyst, deprotonation can occur to form a negatively charged surface, leading to a decoupled electron−proton process, as shown in Figure 7. A very similar deprotonation process was observed recently in the case of the water oxidation reaction at n-SrTiO$_3$.[45]
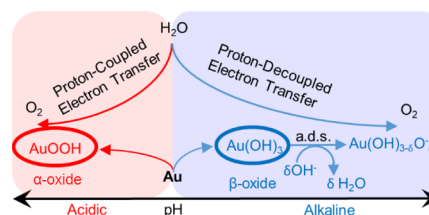
Figure 7. Proposed mechanism for electrocatalytic water oxidation on gold. In the high-pH region, the rate-limited step of oxygen evolution is deprotonation of Au(OH)$_3$ involving a decoupled proton-transfer step.

This concept of surface deprotonation has been confirmed by thermodynamic explanations,[17] simple kinetic models,[46] and experiments.[19,23] β-oxide-Au(OH)$_3$ is also called auric acid, and with a formula of H$_3$AuO$_3$, it is easy to speculate the existence of the (surface) pK_a of Au(OH)$_3$. Here, we do consider the influence of the acid−base characteristics of Au(OH)$_3$ (Au(OH)$_3$ + σOH$^-$ $\rightleftharpoons$ Au(OH)$_{3-\sigma}$O$_\sigma^-$ + σH$_2$O) to the OER process in a high-pH region.

The deprotonation process of β-oxide can be illustrated by rotating disk experiments (Figure 6c,d), showing no significant changes in the OER activity at pH 1 (Figure 6c), while the OER activity at pH 13 massively increases with an increase of the rotation rate (Figure 6d). This indicates that the mass transport of OH$^-$ is not a determining factor for the PCET-OER process at α-oxide but is rate-limiting for the uncoupled OER process on β-oxide. Note that OH$^-$ will likely act as a proton acceptor in the deprotonation process occurring at β-oxide, which explains why mass transport of OH$^-$ is a part of the rate-determining step in the proton-decoupled electron-transfer process. However, we cannot rule out that a part of our observations are due to hydroxide becoming a substrate instead of water under the more alkaline conditions.[47,48]

4. CONCLUSIONS

In summary, we have reassigned the α- and β-reduction peaks of gold to two independent oxides on the basis of our electrochemical and in situ Raman data. It was found that α-oxide is preferentially formed in a low-pH region and β-oxide-Au(OH)$_3$ in a high-pH region. Our studies further revealed that there are two OER mechanisms taking place on a gold oxide surfaces, that is, water splitting to O$_2$ through PCET steps on α-oxide and a path wherein proton transfer and electron transfer are decoupled on β-oxide-Au(OH)$_3$. We believe that our findings are not restricted to gold and offer different insights into how OER occurs at metal oxides.

■ ASSOCIATED CONTENT

Ⓢ Supporting Information

The Supporting Information is available free of charge at https://pubs.acs.org/doi/10.1021/acscatal.0c03548.

> Calculation of onset potential of OER, schematic diagram of the electrochemical setup for SERS measurements, cyclic voltammogram before and after the gold roughing process, recorded reduction potential of the α-peak and β-peak under different rotation rates, cyclic voltammograms in 0.1 M Na$_2$SO$_4$ or NaClO$_4$, cyclic voltammograms of gold at a range of different scan rates, in situ SERS of gold in Ar-saturated HClO$_4$ and H$_2$SO$_4$ solution, oxidative region of cyclic voltammograms at different pH, Tafel analysis under steady-state conditions, and Tafel slopes in different pH solutions (PDF)

■ AUTHOR INFORMATION

Corresponding Author

Dennis G. H. Hetterscheid − *Leiden Institute of Chemistry, Gorlaeus Laboratories, Leiden University, RA Leiden 2300, Netherlands;* ⓘ orcid.org/0000-0001-5640-4416; Email: d.g.h.hetterscheid@chem.leidenuniv.nl

Author

Shengxiang Yang − *Leiden Institute of Chemistry, Gorlaeus Laboratories, Leiden University, RA Leiden 2300, Netherlands;* ⓘ orcid.org/0000-0002-7202-4859

Complete contact information is available at:
https://pubs.acs.org/10.1021/acscatal.0c03548

Notes

The authors declare no competing financial interest.

■ ACKNOWLEDGMENTS

■ REFERENCES

(1) Paets van Troostwijk, A.; Deiman, J. R. Über Die Zerlegung Des Wassers in Brennbare Und Lebensluft Durch Den Elektrischen Funken. *Ann. Phys.* **1790**, *2*, 130−141.

(2) De Levie, R. The Electrolysis of Water. *J. Electroanal. Chem.* **1999**, *476*, 92−93.

(3) McCrory, C. C. L.; Jung, S.; Peters, J. C.; Jaramillo, T. F. Benchmarking Heterogeneous Electrocatalysts for the Oxygen Evolution Reaction. *J. Am. Chem. Soc.* **2013**, *135*, 16977−16987.

(4) Suntivich, J.; May, K. J.; Gasteiger, H. A.; Goodenough, J. B.; Shao-Horn, Y. A Perovskite Oxide Optimized for Oxygen Evolution Catalysis from Molecular Orbital Principles. *Science* **2011**, *334*, 1383−1385.

(5) Browne, M. P.; Sofer, Z.; Pumera, M. Layered and Two Dimensional Metal Oxides for Electrochemical Energy Conversion. *Energy Environ. Sci.* **2019**, *12*, 41−58.

(6) Diaz-Morales, O.; Calle-Vallejo, F.; de Munck, C.; Koper, M. T. M. Electrochemical Water Splitting by Gold: Evidence for an Oxide Decomposition Mechanism. *Chem. Sci.* **2013**, *4*, 2334−2343.

(7) Rossmeisl, J.; Qu, Z.-W.; Zhu, H.; Kroes, G.-J.; Nørskov, J. K. Electrolysis of Water on Oxide Surfaces. *J. Electroanal. Chem.* **2007**, *607*, 83−89.

(8) Conway, B. E. Electrochemical Oxide Film Formation at Noble Metals as a Surface-Chemical Process. *Prog. Surf. Sci.* **1995**, *49*, 331−452.

(9) Burke, L. D.; Lyons, M. E. G. *Modern Aspects of Electrochemistry*; White, R. E., Bockris, J. O. M., Conway, B. E., Eds.; Springer: New York, 1986; Vol. *18*; pp 169−189.

(10) Bond, G. C.; Thompson, D. T. Catalysis by Gold. *Catal. Rev.* **1999**, *41*, 319−388.

(11) Haruta, M. New Generation of Gold catalysts: Nanoporous Foams and Tubes—is Unsupported Gold Catalytically Active? *Chemphyschem* **2007**, *8*, 1911−1913.

(12) Juodkazis, K.; Juodkazytė, J.; Juodienė, T.; Šukienė, V.; Savickaja, I. Alternative View of Anodic Surface Oxidation of Noble Metals. *Electrochim. Acta* **2006**, *51*, 6159−6164.

(13) Tremiliosi-Filho, G.; Dall'Antonia, L. H.; Jerkiewicz, G. Growth of Surface Oxides on Gold Electrodes under Well-defined Potential, Time and Temperature Conditions. *J. Electroanal. Chem.* **2005**, *578*, 1−8.

(14) Gao, X.; Hamelin, A.; Weaver, M. J. Reconstruction at Ordered Au(110)-aqueous Interfaces as Probed by Atomic-resolution Scanning Tunneling microscopy. *Phys. Rev. B* **1991**, *44*, 10983−10986.

(15) Lipkowski, J.; Ross, P. N. *Structure of Electrified Interfaces*; Wiley-VCH: New York, 1993; Vol. 2; p 65.

(16) Weiher, N. *Combined in Situ and Ex Situ Studies of an Electrochemical Interface: Investigation of Anodic Oxide Layers on Gold*; Freie Universitaet: Berlin, 2003; p 13.

(17) Koper, M. T. M. Theory of Multiple Proton-electron Transfer Reactions and its Implications for Electrocatalysis. *Chem. Sci.* **2013**, *4*, 2710−2723.

(18) Frydendal, R.; Busch, M.; Halck, N. B.; Paoli, E. A.; Krtil, P.; Chorkendorff, I.; Rossmeisl, J. Enhancing Activity for the Oxygen

Evolution Reaction: The Beneficial Interaction of Gold with Manganese and Cobalt Oxides. *ChemCatChem* **2015**, *7*, 149−154.

(19) Diaz-Morales, O.; Ferrus-Suspedra, D.; Koper, M. T. M. The Importance of Nickel Oxyhydroxide Deprotonation on its Activity towards Electrochemical Water Oxidation. *Chem. Sci.* **2016**, *7*, 2639−2645.

(20) Giordano, L.; Han, B.; Risch, M.; Hong, W. T.; Rao, R. R.; Stoerzinger, K. A.; Shao-Horn, Y. pH Dependence of OER Activity of Oxides: Current and Future Perspectives. *Catal. Today* **2016**, *262*, 2−10.

(21) Grimaud, A.; Diaz-Morales, O.; Han, B.; Hong, W. T.; Lee, Y.-L.; Giordano, L.; Stoerzinger, K. A.; Koper, M. T. M.; Shao-Horn, Y. Activating Lattice Oxygen Redox Reactions in Metal Oxides to Catalyse Oxygen Evolution. *Nat. Chem.* **2017**, *9*, 457−465.

(22) Stoerzinger, K. A.; Rao, R. R.; Wang, X. R.; Hong, W. T.; Rouleau, C. M.; Shao-Horn, Y. The Role of Ru Redox in pH-Dependent Oxygen Evolution on Rutile Ruthenium Dioxide Surfaces. *Chem* **2017**, *2*, 668−675.

(23) Trześniewski, B. J.; Diaz-Morales, O.; Vermaas, D. A.; Longo, A.; Bras, W.; Koper, M. T.; Smith, W. A. In Situ Observation of Active Oxygen Species in Fe-containing Ni-based Oxygen Evolution Catalysts: the Effect of pH on Electrochemical Activity. *J. Am. Chem. Soc.* **2015**, *137*, 15112−15121.

(24) Kuo, D.-Y.; Kawasaki, J. K.; Nelson, J. N.; Kloppenburg, J.; Hautier, G.; Shen, K. M.; Schlom, D. G.; Suntivich, J. Influence of Surface Adsorption on the Oxygen Evolution Reaction on IrO$_2$ (110). *J. Am. Chem. Soc.* **2017**, *139*, 3473−3479.

(25) Huang, Z.-F.; Wang, J.; Peng, Y.; Jung, C.-Y.; Fisher, A.; Wang, X. Design of Efficient Bifunctional Oxygen Reduction/Evolution Electrocatalyst: Recent Advances and Perspectives. *Adv. Energy Mater.* **2017**, *7*, 1700544.

(26) Gerken, J. B.; McAlpin, J. G.; Chen, J. Y. C.; Rigsby, M. L.; Casey, W. H.; Britt, R. D.; Stahl, S. S. Electrochemical Water Oxidation with Cobalt-based Electrocatalysts from pH 0-14: the Thermodynamic Basis for Catalyst Structure, Stability, and Activity. *J. Am. Chem. Soc.* **2011**, *133*, 14431−14442.

(27) Diaz-Morales, O.; Hersbach, T. J. P.; Hetterscheid, D. G. H.; Reek, J. N. H.; Koper, M. T. M. Electrochemical and Spectroelectrochemical Characterization of an Iridium-Based Molecular Catalyst for Water Splitting: Turnover Frequencies, Stability, and Electrolyte Effects. *J. Am. Chem. Soc.* **2014**, *136*, 10432−10439.

(28) de Ruiter, J. M.; Purchase, R. L.; Monti, A.; van der Ham, C. J. M.; Gullo, M. P.; Joya, K. S.; D'Angelantonio, M.; Barbieri, A.; Hetterscheid, D. G. H.; de Groot, H. J. M.; Buda, F. Electrochemical and Spectroscopic Study of Mononuclear Ruthenium Water Oxidation Catalysts: A Combined Experimental and Theoretical Investigation. *ACS Catal.* **2016**, *6*, 7340−7349.

(29) Lai, S. C. S.; Kleyn, S. E. F.; Rosca, V.; Koper, M. T. M. Mechanism of the Dissociation and Electrooxidation of Ethanol and Acetaldehyde on Platinum as Studied by SERS. *J. Phys. Chem. C* **2008**, *112*, 19080−19087.

(30) Gao, P.; Gosztola, D.; Leung, L.-W. H.; Weaver, M. J. Surface Enhanced Raman scattering at Gold Electrodes-dependence on Electrochemical Pretreatment Conditions and Comparisons with Silver. *J. Electroanal. Chem.* **1987**, *233*, 211−222.

(31) Burke, L. D.; Nugent, P. F. The Electrochemistry of Gold: I the Redox Behaviour of the Metal in Aqueous Media. *Gold Bull.* **1997**, *30*, 43−53.

(32) Pourbaix, M. *Atlas of Electrochemical Equilibria in Aqueous Solution*; National Association of Corrosion Engineers: Houston, TX, 1974; Vol. 2; p 644.

(33) Burke, L. D.; Buckley, D. T.; Morrissey, J. A. Novel View of the Electrochemistry of Gold. *Analyst* **1994**, *119*, 841−845.

(34) Peuckert, M.; Coenen, F. P.; Bonzel, H. P. On the Surface Oxidation of a Gold Electrode in 1N H$_2$SO$_4$ Electrolyte. *Surf. Sci.* **1984**, *141*, 515−532.

(35) Weiher, N.; Willneff, E. A.; Figulla-Kroschel, C.; Jansen, M.; Schroeder, S. L. M. Extended X-ray Absorption Fine-structure (EXAFS) of a Complex Oxide Structure: a Full Multiple Scattering Analysis of the Au L-3-edge EXAFS of Au$_2$O$_3$. *Solid State Commun.* **2003**, *125*, 317−322.

(36) Lohrengel, M. M.; Schultze, J. W. Electrochemical Properties of Anodic Gold Oxide Layers—I: Potentiostatic Oxide Growth and Double Layer Capacity. *Electrochim. Acta* **1976**, *21*, 957−965.

(37) Burke, L. D.; McRann, M. Thick Oxide Growth on Gold in Base. *J. Electroanal. Chem. Interfacial Electrochem.* **1981**, *125*, 387−399.

(38) Doyle, R. L.; Lyons, M. E. G. The Mechanism of Oxygen Evolution at Superactivated Gold Electrodes in Aqueous Alkaline Solution. *J. Solid State Electrochem.* **2014**, *18*, 3271−3286.

(39) Kawamoto, D.; Ando, H.; Ohashi, H.; Kobayashi, Y.; Honma, T.; Ishida, T.; Tokunaga, M.; Okaue, Y.; Utsunomiya, S.; Yokoyama, T. Structure of a Gold(III) Hydroxide and Determination of Its Solubility. *Bull. Chem. Soc. Jpn.* **2016**, *89*, 1385−1390.

(40) Yeo, B. S.; Klaus, S. L.; Ross, P. N.; Mathies, R. A.; Bell, A. T. Identification of Hydroperoxy Species as Reaction Intermediates in the Electrochemical Evolution of Oxygen on Gold. *Chemphyschem* **2010**, *11*, 1854−1857.

(41) Desilvestro, J.; Weaver, M. J. Surface Structural Changes during Oxidation Gold Electrodes in Aqueous Media as Detected Using Surface Enhanced Raman Spectroscopy. *J. Electroanal. Chem.* **1986**, *209*, 377−386.

(42) Liu, K.; Chen, T.; He, S.; Robbins, J. P.; Podkolzin, S. G.; Tian, F. Observation and Identification of an Atomic Oxygen Structure on Catalytic Gold Nanoparticles. *Angew. Chem., Int. Ed. Engl.* **2017**, *56*, 12952−12957.

(43) Rossmeisl, J.; Logadottir, A.; Nørskov, J. K. Electrolysis of Water on (oxidized) Metal Surfaces. *Chem. Phys.* **2005**, *319*, 178−184.

(44) Kwon, Y.; Lai, S. C. S.; Rodriguez, P.; Koper, M. T. M. Electrocatalytic Oxidation of Alcohols on Gold in Alkaline Media: Base or Gold catalysis? *J. Am. Chem. Soc.* **2011**, *133*, 6914−6917.

(45) Chen, X.; Aschaffenburg, D. J.; Cuk, T. Selecting between Two Transition States by which Water Oxidation Intermediates Decay on an Oxide Surface. *Nat. Catal.* **2019**, *2*, 820−827.

(46) Koper, M. T. M. Volcano Activity Relationships for Proton-coupled Electron Transfer Reactions in Electrocatalysis. *Top. Catal.* **2015**, *58*, 1153−1158.

(47) Kafizas, A.; Ma, Y.; Pastor, E.; Pendlebury, S. R.; Mesa, C.; Francàs, L.; Le Formal, F.; Noor, N.; Ling, M.; Sotelo-Vazquez, C.; Carmalt, C. J.; Parkin, I. P.; Durrant, J. R. Water Oxidation Kinetics of Accumulated Holes on the Surface of a TiO$_2$ Photoanode: A Rate Law Analysis. *ACS Catal.* **2017**, *7*, 4896−4903.

(48) Imanishi, A.; Okamura, T.; Ohashi, N.; Nakamura, R.; Nakato, Y. Mechanism of Water Photooxidation Reaction at Atomically Flat TiO$_2$ (rutile) (110) and (100) Surfaces: Dependence on Solution pH. *J. Am. Chem. Soc.* **2007**, *129*, 11569−11578.